Cell Biol Toxicol (2025) 41:55
https://doi.org/10.1007/s10565-025-10005-x

RESEARCH

# Neutrophil-derived heparin-binding protein increases endothelial permeability in acute lung injury by promoting TRIM21 and the ubiquitination of P65

**Jian Zhang · Yong Cao · Wenqi Shu · Senxiao Dong · Yini Sun · Xiaochun Ma**

Received: 1 October 2024 / Accepted: 20 February 2025


**Abstract** Acute lung injury (ALI), which poses a significant public health threat, is commonly caused by sepsis. ALI is associated with permeability and glycolysis changes in pulmonary microvascular endothelial cells. Our study demonstrates that heparin-binding protein (HBP), released from neutrophils during sepsis, exacerbates endothelial permeability and glycolysis, thereby triggering ALI. Through coimmunoprecipitation and mass spectrometry, TRIM21 was identified as a HBP interaction partner. Notably, HBP enhances the protein stability of TRIM21 by inhibiting K48 ubiquitination. TRIM21 binds to and promotes K63-linked ubiquitination of P65, facilitating its nuclear translocation. TRIM21 regulates HPMEC permeability and glycolysis in a manner dependent on P65 nuclear translocation. HBP stabilizes TRIM21 and enhances TRIM21 interactions with P65. Rescue experiments conducted in vivo and in vitro demonstrate that modulation of endothelial permeability and glycolysis by HBP is predominantly mediated through the TRIM21-P65 axis. Our results suggest that targeting the HBP/TRIM21/P65 axis is a novel therapeutic strategy to ameliorate ALI.

**Keywords** Heparin-binding protein · Acute lung injury · TRIM21 · P65 · Ubiquitination

## Introduction

ALI is a life-threatening noncardiogenic pulmonary edema caused by intrapulmonary or extrapulmonary factors, leading to acute hypoxemic respiratory failure (Meyer et al. 2021). The hallmark pathological characteristics of ALI include widespread alveolar damage, elevated vascular permeability, and neutrophil infiltration, all of which synergistically lead to compromised gas exchange and respiratory impairment. As the condition deteriorates, ALI progresses to the more severe acute respiratory distress syndrome (ARDS). Sepsis, which is defined as "a life-threatening organ dysfunction caused by a host's dysfunctional response to infection," is the most common cause of ARDS (Evans et al. 2021). The inflammatory cascade induced by sepsis leads to extensive damage to endothelial and epithelial cells, further aggravating the breakdown of the alveolar-capillary barrier and the development of pulmonary edema. Despite advances in medical technology, the in-hospital mortality rate for sepsis-associated ARDS is as high as 40% (Bellani et al. 2016). Sepsis-associated ARDS significantly impacts patient outcomes and

**Supplementary Information** The online version contains supplementary material available at https://doi.org/10.1007/s10565-025-10005-x.

J. Zhang · Y. Cao · W. Shu · S. Dong · Y. Sun · X. Ma (✉)
Department of Critical Care Medicine, The First Affiliated Hospital, China Medical University, North Nanjing Street 155, Shenyang 110001, Liaoning Province, People's Republic of China
e-mail: maxc_cmu@sina.com

Published online: 05 March 2025

imposes a substantial burden on patients, their families, and society.

The endothelial cell (EC) monolayer serves as a critical barrier, regulating the exchange of fluids, nutrients, and cells between the bloodstream and interstitial spaces (Dalal et al. 2020; Marziano et al. 2021). The integrity of human pulmonary microvascular ECs (HPMECs) is essential for maintaining lung function. Both pathogen-associated molecular patterns and damage-associated molecular patterns compromise endothelial integrity, increase vascular permeability, and contribute to lung injury during sepsis (Joffre et al. 2020). Moreover, ECs transform rapidly from a quiescent state to a highly inflammatory and activated state. This process is driven by dynamic changes in glycolysis during sepsis and inflammation (Clyne 2021). Glycolysis plays a significant role in the progression of ALI (Li et al. 2023a). Thus, EC permeability and glycolysis are promising therapeutic targets for managing lung injury.

Polymorphonuclear neutrophils (PMNs) are crucial for immune defense. PMNs modulate ALI via degranulation, phagocytosis, and cellular infiltration. HBP, also known as AZU1, is synthesized and stored within secretory vesicles and azurophilic granules of PMNs. Upon activation by antigens, cytokines, or other inflammatory mediators during sepsis, HBP is released into the bloodstream. Thus, HBP is a biomarker for infection severity and the transition to severe sepsis (Yang et al. 2019). Our previous findings demonstrate that HBP interacts with endothelial Transforming growth factor-β receptor type 2, activating the TGF-β and Rho–ROCK signaling pathways and facilitating cytoskeletal remodeling, which culminate in ALI (Liu et al. 2022). However, the regulatory effects of HBP on the endothelial barrier, glycolysis, and endothelial dysfunction are unclear, underscoring the need for more studies.

To further elucidate the role and underlying mechanisms of HBP in ECs, our preliminary studies identified TRIM21 as a potential interacting protein through Co-IP and LC–MS analyses. TRIM21, a member of the Tripartite motif (TRIM) family, regulates crucial cellular processes including innate immunity, transcription, and autophagy. Notably, increased TRIM21 expression has been linked to a variety of autoimmune and inflammatory disorders (Holwek et al. 2023). Recent findings suggest that TRIM21 may promote Gasdermin D-mediated pyroptosis, positioning it as a potential therapeutic target for inflammation-related diseases (Gao et al. 2022). Nevertheless, the specific role of TRIM21 in HBP-mediated endothelial dysfunction remains to be defined.

P65, also referred to as RelA, is a critical component of the NF-κB family. Conditions such as ALI/ARDS, and chronic obstructive pulmonary disease are notably linked with the dysregulated activation of the NF-κB pathway (Alharbi et al. 2021; Millar et al. 2022). Previous studies have demonstrated that HBP amplifies NF-κB pathway-mediated transcription of inflammatory genes in macrophages during sepsis (Lu et al. 2021). However, the specific regulatory mechanisms through which HBP modulates P65 transcriptional activity remain to be elucidated.

The objective of this study was to determine the relationship between septic PMNs and endothelial dysfunction. Our results demonstrate that HBP released from septic PMNs enhances EC permeability and influences glycolytic processes. Notably, unfractionated heparin effectively reduces endothelial damage induced by HBP. Moreover, the functional roles of TRIM21 and P65 were evaluated in the context of HBP-induced lung injury; the potential role of interactions between TRIM21 and P65 in modulating endothelial permeability and glycolysis in ALI were investigated. The novel pathways and mechanisms through which neutrophil-derived HBP mediates endothelial damage were elucidated and new therapeutic targets for the management of ALI were identified.

## Materials and methods

### Chemicals and reagents

MG132 and JSH-23 were obtained from MedChemExpress. Cycloheximide (CHX) was sourced from Sigma-Aldrich, and recombinant HBP was procured from Novoprotein. Transfection reagents included Higene (Applygen Technology) and Lipo3000 (Life Technologies Corporation).

### Cell culture treatment and transfection

HPMECs were acquired from Tongpai technology and cultured in Dulbecco's modifed Eagle's medium

supplemented with 10% fetal bovine serum. After 2–3 days, they reached 80–90% confluence and were passaged using 0.25% trypsin. Cells were passaged at 80–90% confluence using 0.25% trypsin,and cells within 40 passages were used for all experiments. HPMECs were confirmed to be CD31-positive by immunofluorescence staining, ensuring the endothelial identity. In the cell experiments, the HBP group was treated with 1 μg/mL recombinant HBP protein for 24 h.

For transfection experiments, flag-HBP (MiaoLingBio, China),myc-TRIM21plasmids (MiaoLingBio, China), HA-Ub(MiaoLingBio, China), HA-Ub K48(MiaoLingBio, China), HA-Ub K63(MiaoLingBio, China) and corresponding empty vector were transfected into cells using transfection reagents according to the manufacturer's instructions. After 48 h of culture post-transfection, cells were uesd for subsequent experiments. TRIM21 gene silencing was performed in HPMECs by si-TRIM21(Haixing Biotech), with both siRNA and scrambled siRNA stock concentrations of 20 μM and working concentrations of 50–100 nM. Negative control (NC) included scrambled siRNA transfections. After 48 h, levels of TRIM21 proteins were detected by immunoblotting to verify transfection efficiency (sFigure 1). Subsequently, TRIM21 was knocked down using TRIM21 siRNA1.

## Clinical data collection and human neutrophils isolation

Clinical data on plasma HBP concentrations were collected from sepsis patients, both with and without ARDS, in the intensive care unit of the First Affiliated Hospital of China Medical University. Blood samples were collected in EDTA-coated tubes for neutrophil isolation isolation from healthy donors and sepsis patients who provided informed consent. All clinical data collection and experiments were conducted in accordance with the approval granted by the Ethics Committee of the First Affiliated Hospital of China Medical University (Approval Number: 2023–157). The inclusion criteria for participants are detailed in the Supplementary Materials.

Neutrophils were isolated using density gradient centrifugation by a commercial neutrophil extraction kit(P9040, Solarbio). Viability was assessed by Trypan Blue exclusion, which showed that more than 90% of the cells were viable. Cells were cultured in RPMI 1640 supplemented with 10% FBS.

## Animal experiments and lung injury model

C57/BL male mice, aged 6–8 weeks, were obtained from Liaoning Changsheng Biological Company. The mice were housed under a clean environment with sufficient water and food, maintaining a normal circadian rhythm. Mice were anesthetized with isoflurane and euthanized by cervical dislocation at the end of the experiment. All procedures were approved by the Institutional Animal Care and Use Committee of China Medical University(Approval Number KT20240002).

Based on preliminary experimental results, intravenous injection of 25 μg recombinant HBP protein was identified as the minimum dose required to induce lung injury in mice (sFig 2A, B). Therefore, this study employed 25 μg recombinant HBP administered via tail vein injection to establish the HBP-induced lung injury model. Mice were subjected to HBP treatment for 24 h (HBP group), while the control group received an equal volume of saline via tail vein injection. Each group consisted of five mice. To establish a LPS-induced acute lung injury model, mice were intratracheally administered 5 mg/kg LPS (2630, Sigma) in 50 μl saline for 24 h, with control mice receiving saline alone. Each group consisted of five mice.

## Co-culture experiments

HPMECs and neutrophils were co-cultured in a Transwell system (0.4 μm pore size, 3413, Corning). HPMECs were seeded in the bottom chamber and neutrophils (5 × 10^5 cells) in the upper chamber. After 24 h, HPMEC samples were collected. To measure TEER and FITC-dextran leakage, HPMECs were seeded in the upper chambers and PMNs were placed in the lower chambers.

## Enzyme-linked immunosorbent assay (Elisa)

HBP levels in EC supernatants were measured using a commercial ELISA kit (SEB461Hu, Cloud-Clone Corp, Wuhan, China). Samples were diluted 100-fold, and 100 μL of each was added to antibody-coated wells, followed by incubation at 37 °C for 90 min. After washing, 100 μL of biotin-labeled detection antibody was added and incubated at 37 °C for 60 min. Following another wash, 100 μL

of HRP-avidin conjugate was added and incubated at 37 °C for 30 min. After a final wash, 90 μL of TMB substrate was added for color development at 37 °C in the dark for 15–20 min. The reaction was stopped with 50 μL of stop solution, and absorbance at 450 nm was measured using a microplate reader. HBP concentrations were calculated using a standard curve.

### Western blot

Protein lysates were prepared using RIPA buffer, and protein concentrations were determined by BCA assay. Samples (20–40 μg protein) were resolved by SDS-PAGE, transferred to PVDF membranes, and probed with the following primary antibodies: ZO-1 (21,773–1-AP, Proteintech, 1:5000), occludin (27,260–1-AP, Proteintech, 1:5000), claudin-5 (29,767–1-AP, Proteintech, 1:5000), TRIM21 (12,108–1-AP, Proteintech, 1:5000), P65 (80,979–1-RR, Proteintech, 1:1000), β-actin (81,115–1-RR, Proteintech, 1:10,000), Flag (66,008–4-Ig, Proteintech, 1:1000), Myc (16,286–1-AP, Proteintech, 1:5000), Histone 3 (17,168–1-AP, Proteintech, 1:10,000), HBP (MAB2200, R&D Systems, 1:1000), Ub (10,201–2-AP, Proteintech, 1:1000), K63-Ub (ab179434, Abcam, 1:1000), HA (51,064–2-AP, Proteintech, 1:10,000), ROCK2 (21,645–1-AP, Proteintech, 1:5000), ROCK1 (21,850–1-AP, Proteintech, 1:5000), Phospho-NF-κB p65 (Ser536) (80,379–2-RR, Proteintech, 1:1000), and Rho (mAb A4855, Abclonal, 1:1000). Gels were visualized using enhanced chemiluminescence.

### Co-immunoprecipitation(Co-IP) and mass spectrometry analysis

Cells or lung tissue of mice were lysed in IP lysis (0.25% Sodium deoxycholate, 1 mM Tris–HCl 7.4, 0.5 M EDTA, 1% Triton-X 100, 1% NP40, 150 mM Nacl) containing protease inhibitors. After 30 min on ice, the lysate was centrifuged, and protein concentration was measured using a BCA assay. An aliquot of supernatant was set aside as input. The remaining lysate (1000 μg protein) was incubated with primary antibodies at 4 °C for 2 h, followed by overnight incubation with protein A/G magnetic beads (K1305, Apexbio, USA). The beads were then washed three times with IP buffer and proteins were boiled in 2 × SDS-PAGE buffer at 100 °C for 10 min.

The proteins were separated by SDS-PAGE and the relevant bands were excised, digested into peptides, and analyzed by LC–MS (PTM BIO). Data were processed with Proteome Discoverer 2.4 to identify protein interactions.

### FITC-dextran leakage assay

Confluent layers of HPMECs in Transwell inserts were incubated with 1 mg/ml FITC-dextran to evaluate barrier permeability. After one hour of exposure, samples collected from the lower chamber were analyzed for fluorescence intensity to quantitatively assess the integrity of the endothelial barrier.

### Transendothelial electrical resistance (TEER) measurement

TEER was assessed using a millicell-ERS instrument (Merck Millipore). ECs were cultured to confluence within Transwell inserts, and the culture medium was refreshed just prior to the measurements. Inserts were allowed to stabilize at 25 °C for 30 min before TEER values were recorded. During stabilization, the system was kept in a constant-temperature environment to ensure stable conditions. The inserts were undisturbed, allowing the cell layers and medium to equilibrate and eliminate any initial disturbances. This step minimized external influences and ensured a steady state before measurements. To account for background resistance, control values obtained from blank inserts were subtracted from those of the experimental groups. Subsequently, TEER values were normalized to the membrane surface area, resulting in measurements expressed as ohms*$cm^2$. This normalization provides a quantitative assessment of endothelial barrier integrity.

### Lactate measurement

Lactate concentrations in bronchoalveolar lavage fluid (BALF) and cell culture supernatants were determined using a Micro Lactate Assay Kit (KTB1100, Abbkine) in accordance with the manufacturer's instructions.

### Extracellular acidification rate (ECAR)

ECAR was measured using an XF24 extracellular flux analyzer (Seahorse Bioscience). HPMECs at a density of 5 × 10^4 cells per well were plated on an XF24 plate. ECAR measurements were sequentially performed following the addition of glucose, oligomycin, and 2-deoxy-D-glucose (2-DG). Data analysis was conducted using Seahorse Wave software, which processed ECAR readings and evaluatedglycolysis capability following the manufacturer's protocol.

### Immunofluorescence staining

Cells were cultured on glass slides, followed by fixation with 4% paraformaldehyde and permeabilization using 0.1% Triton X-100 for 10 min. To prevent nonspecific binding, cells were blocked with 2% bovine serum albumin. Cells were incubated with primary antibodies against HBP (MAB461Hu24,Cloud-clone,1:100) and TRIM21(12,108–1-AP, proteintech,1:100) at 4 °C overnight. Subsequently, they were exposed to appropriate fluorescence-tagged secondary antibodies. Nuclei were stained with DAPI(G1012, servicebio) for 5 min. Fluorescence images were acquired using a Nikon A1 laser confocal microscope to evaluate protein localization.

### Protein stability and degradation assay

To assess protein synthesis inhibition, HPMEC cells overexpressing HBP or a control plasmid were treated with 100 μg/mL CHX 24 h post-transfection. Total proteins were collected at different times for Western blot analysis. For protein degradation assay, cells were treated with 10 μM MG132, a proteasome inhibitor, or DMSO for the control group, and proteins were subsequently extracted for Western blotting to evaluate the effects on proteasomal degradation.

### Quantitative real-time PCR (qRT-PCR)

Total RNA was extracted from HPMECs using a RNA extraction kit and quantified via spectrophotometry. Complementary DNA was synthesized using a reverse transcription master mix, and qPCR was performed with β-actin serving as an internal control. Primer information is detailed in Supplementary Table S1.

### Lung wet-to-dry (W/D) ratio

Fresh right lung tissue was weighed and then dried at 68 °C until constant weight was achieved. Lung W/D ratio was calculated to assess pulmonary tissue exudation.

### HE staining and lung inflammation score

Lung tissue was fixed in 4% paraformaldehyde, embedded in paraffin, and sectioned at 4 μm thickness. Sections were deparaffinized, rehydrated, and stained with hematoxylin and eosin for histological examination under a microscope. Lung injury was evaluated based on histopathological parameters including pulmonary edema, inflammation, hemorrhage, atelectasis, and hyaline membrane formation. Each parameter was scored semi-quantitatively from 0 to 4: 0 (no injury), 1 (< 25% involvement), 2 (25%−50%), 3 (50%−75%), and 4 (> 75%). The total injury score was the sum of all parameter scores. To reduce bias, 10 high-power fields were randomly selected for each animal, and scoring was performed independently by two investigators, with the average score representing the final lung injury score.

### Evans blue leakage assay

Mice were injected intravenously with 0.5% Evans Blue dye. After one hour, pulmonary vasculature was cleared, and lung tissue was harvested and homogenized in formamide (1 mL per 100 mg tissue). Following incubation at 37 °C for 24 h and centrifugation, the supernatant's absorbance was measured to determine Evans Blue dye leakage, using a standard curve for quantification.

### Isolation of primary pulmonary endothelial cells from mice

Primary pulmonary endothelial cells from mice were isolated using magnetic bead separation. Fresh lung tissue was first thoroughly washed with basal medium, then cut into small pieces and incubated in collagenase solution at 37 °C for 45 min. Next, 15μL of pre-incubated anti-CD31 antibody(553,370, BD)-conjugated magnetic beads(11,035, Thermo Fisher Scientific) were added per milliliter of cell suspension and incubated at 4 °C for 20 min. After discarding

the cell suspension, the magnetic beads were washed with medium to obtain purified primary pulmonary endothelial cells.

### Adenoviral vector infection

An adenoviral vector was purchased from Hanbio Tech (Shanghai, China). To knock down TRIM21 expression in the lung tissue of C57BL/6 mice, we employed HBAAV2/6-m-trim21 shRNA1-EGFP (shTRIM21), with HBAAV2/6-EGFP NC serving as the control vector. The vector, administered intratracheally at a dose of 5×10^10 viral genomes in 0.1 μL, achieved stable expression three weeks post-administration.

Wild-type mice without adenovirus transfection, mice infected with shNC adenovirus, and mice infected with shTRIM21 adenovirus were designated as WT, shNC, and shTRIM21 groups, respectively. Each group consisted of five mice. After receiving HBP or LPS treatment for the corresponding duration, the mice were sacrificed for subsequent experiments.

### Statistical analysis

Data were analyzed using SPSS Version 23 and GraphPad Prism 9. Experimental results are reported as mean ± standard deviation (SD). For comparisons between two groups, the Student's t-test was applied. Differences among three or more groups were analyzed using one-way analysis of variance (ANOVA), with Bonferroni's method for inter-group comparisons. $P < 0.05$ was considered statistically significant.

## Results

### Neutrophil-derived HBP from septic patients causes HPMEC barrier disruption and promotes glycolysis

To determine the correlation between HBP secretion by neutrophils and lung injury, we analyzed plasma HBP concentrations in patients with sepsis. Plasma HBP levels were significantly higher in sepsis patients with ARDS compared to the levels in sepsis patients without lung injury (Fig. 1A), indicating a strong association between elevated HBP levels and lung injury in sepsis. HPMECs were cocultured with neutrophils in a Transwell system. HBP levels were significantly higher in cocultures with sepsis-derived PMNs compared to cocultures with healthy PMNs (Fig. 1B). Endothelial integrity and permeability were assessed using TEER and FITC-dextran leakage assays, respectively. No significant differences in endothelial integrity and permeability were detected between the control group and the healthy PMNs coculture group (Fig. 1C, D). However, TEER value significantly decreased and FITC–dextran leakage significantly increased in HPMECs cocultured with sepsis PMNs compared with ECs cocultured with healthy PMNs (Fig. 1C, D). Furthermore, the expression of the tight junction proteins, ZO-1, occludin, and claudin-5, decreased in the sepsis PMN coculture group (Fig. 1E, F). Extracellular acidification rates and lactate production were measured to determine the effects of HBP on glycolysis in ECs. Both glycolytic capacity and lactate levels were significantly elevated in the sepsis PMN coculture group compared to the corresponding parameters in the healthy PMN group (Fig. 1G-I).

Heparin is a nonspecific HBP antagonist that can bind to HBP and inhibit its function (Bentzer et al. 2016). Heparin did not alter TEER value and FITC–dextran leakage in normal HPMECs but improved both parameters in HPMECs cocultured with sepsis PMNs (Fig. 1J, K). Western blot analysis showed that heparin restored the decrease in tight junction proteins induced by PMNs (Fig. 1L, M). No changes in glycolytic activity and lactate levels were detected between the control group and ECs treated with heparin alone. However, both glycolysis and lactate production were reduced in ECs cocultured with sepsis PMNs and heparin compared to HPMECs cocultured with sepsis PMNs (Fig. 1N–P). These findings suggest that heparin effectively mitigates HBP-mediated increases in HPMEC permeability and glycolysis induced by septic PMNs.

### Recombinant HBP increases EC permeability and glycolysis, leading to ALI

HBP protein was used in in vivo and in vitro experiments to determine the direct effects of HBP on HPMECs. TEER values decreased, FITC–dextran leakage increased, tight junction protein expression decreased, glycolytic capacity increased, and lactate

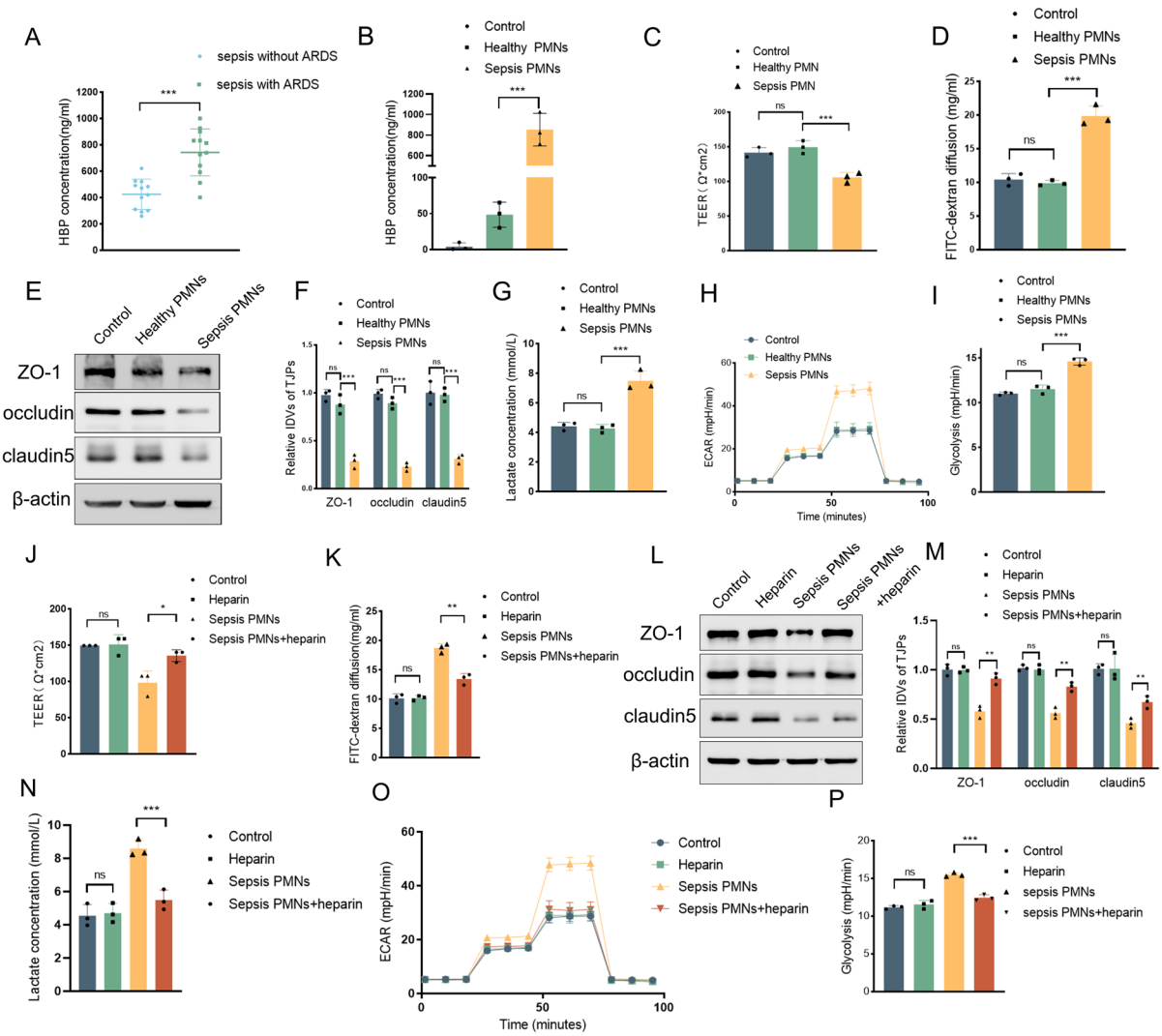


**Fig. 1** HBP secreted by sepsis PMNs disrupts EC barrier and promotes endothelial glycolysis. **A** Plasma HBP levels in sepsis patients with and without ARDS. Data are represented as mean ± SD, n = 12, ***$P < 0.001$. **B** HBP concentrations in EC supernatants from co-cultures with sepsis and healthy PMNs. Data are represented as mean ± standard deviation, n = 3, ***$P < 0.001$. **C, D** TEER values and FITC-dextran leakage in ECs co-cultured with sepsis and healthy PMNs. **E, F** Expression of tight junction proteins in ECs co-cultured with sepsis and healthy PMNs, analyzed by Western blot. Data are represented as mean ± standard deviation, n = 3, ***$P < 0.001$. **G-I** ECAR, lactate production, and glycolysis in ECs co-cultured with sepsis and healthy PMNs, with data represented as mean ± SD, n = 3, ***$P < 0.001$. **J, K** Effects of sepsis PMNs co-culturing with heparin on the TEER values and FITC-dextran leakage. **L, M** Effects of heparin on tight junction protein expression in ECs co-cultured with sepsis PMNs. Data are represented as mean ± SD, n = 3, **$P < 0.01$. **N-P** ECAR, lactate production, and glycolysis in ECs co-cultured with sepsis PMNs and heparin. Data are represented as mean ± SD, n = 3, ***$P < 0.001$

levels increased in ECs treated with 1 μg/ml HBP for 24 h (Fig. 2A–G). Intravenous administration of HBP into the tail vein of mice induced severe lung damage, as evidenced by HE staining and increased histopathological scores (Fig. 2H, I). HPMEC permeability, which was assessed by lung W/D ratios and Evans blue dye extravasation, increased significantly in the HBP-treated mice compared with permeability

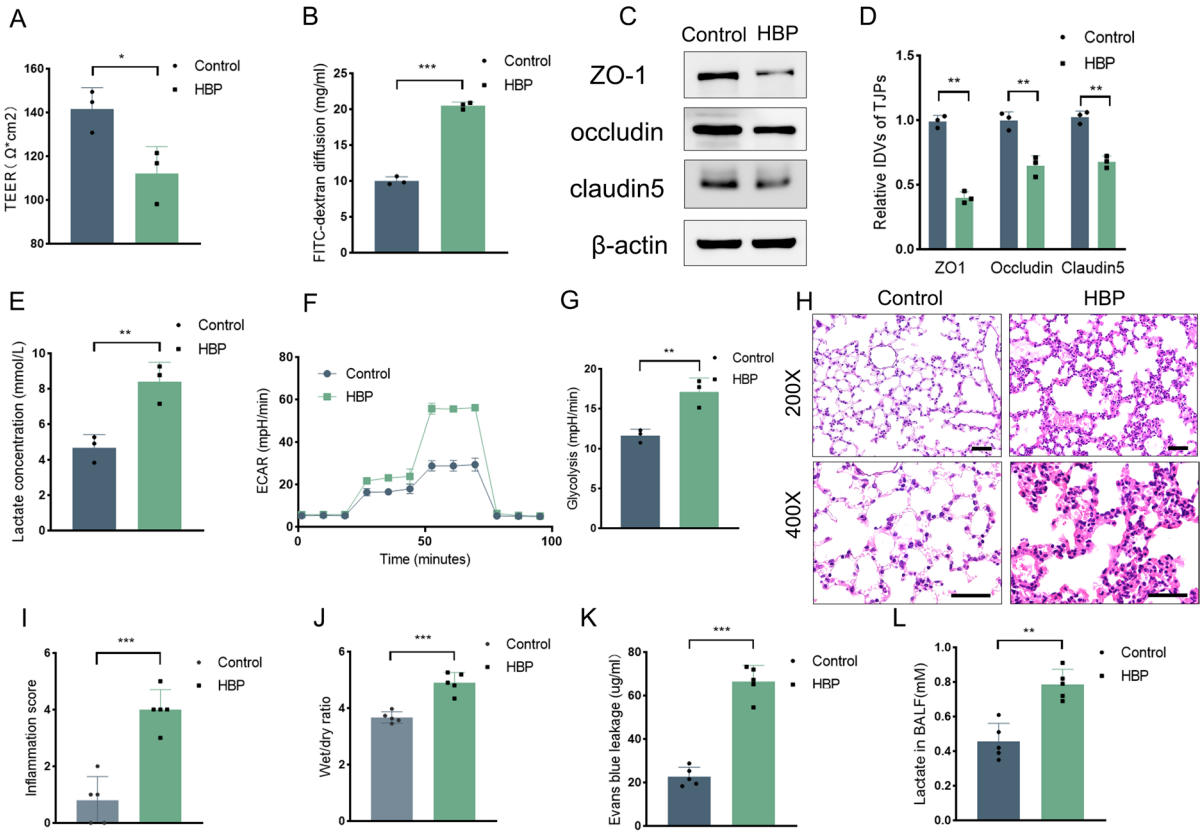


**Fig. 2** HBP directly increases endothelial permeability and glycolysis, leading to ALI. **A, B** TEER values and FITC-dextran leakage in ECs treated with purified HBP protein. **C, D** Tight junction protein expression in HBP-treated ECs, determined by Western blot. Data are represented as mean ± SD, n = 3, $^{**}P < 0.01$. **E–G** ECAR, lactate production, and glycolysis in HBP-treated ECs, represented as mean ± SD, n = 3, $^{**}P < 0.01$. **H, I** HE staining of lung tissues from mice treated with HBP, indicating injury severity, scale bar: 50 μm. Data are represented as mean ± SD, n = 5, $^{***}P < 0.001$. **J-L** Lung W/D ratio, Evans Blue leakage, and BALF lactate content in HBP-treated mice. Data are represented as mean ± SD, n = 5, $^{**}P < 0.01$, $^{***}P < 0.001$

in control mice (Fig. 2J, K). Lactate levels in BALF were quantified to assess glycolysis; lactate concentrations were higher in the HBP group (Fig. 2L). These findings confirmed the induction of increased HPMEC permeability and glycolysis by HBP, thereby exacerbating ALI.

## HBP interacts with TRIM21 and increases its protein stability

Secreted proteins can interact with intracellular proteins of receptor cells and exert different biological functions. Using coimmunoprecipitation and mass spectrometry, we identified potential target proteins of HBP in HPMECs overexpressing HBP. Seventy-eight interacting proteins were identified, and TRIM21 had the highest score (sFig 3A,B). Stimulation of HPMECs with recombinant HBP protein followed by Co-IP experiments confirmed the endogenous interaction between HBP and TRIM21 in HPMECs (Fig. 3A). Immunofluorescence analysis revealed colocalization of HBP and TRIM21 in the cytoplasm (Fig. 3B). Interestingly, while qRT–PCR indicated that HBP overexpression did not alter TRIM21 mRNA levels (Fig. 3C), TRIM21 protein levels increased significantly (Fig. 3D). To explore this discrepancy, protein synthesis was inhibited with CHX. HBP overexpression prolonged TRIM21 protein stability (Fig. 3E). Treatment with the proteasome inhibitor

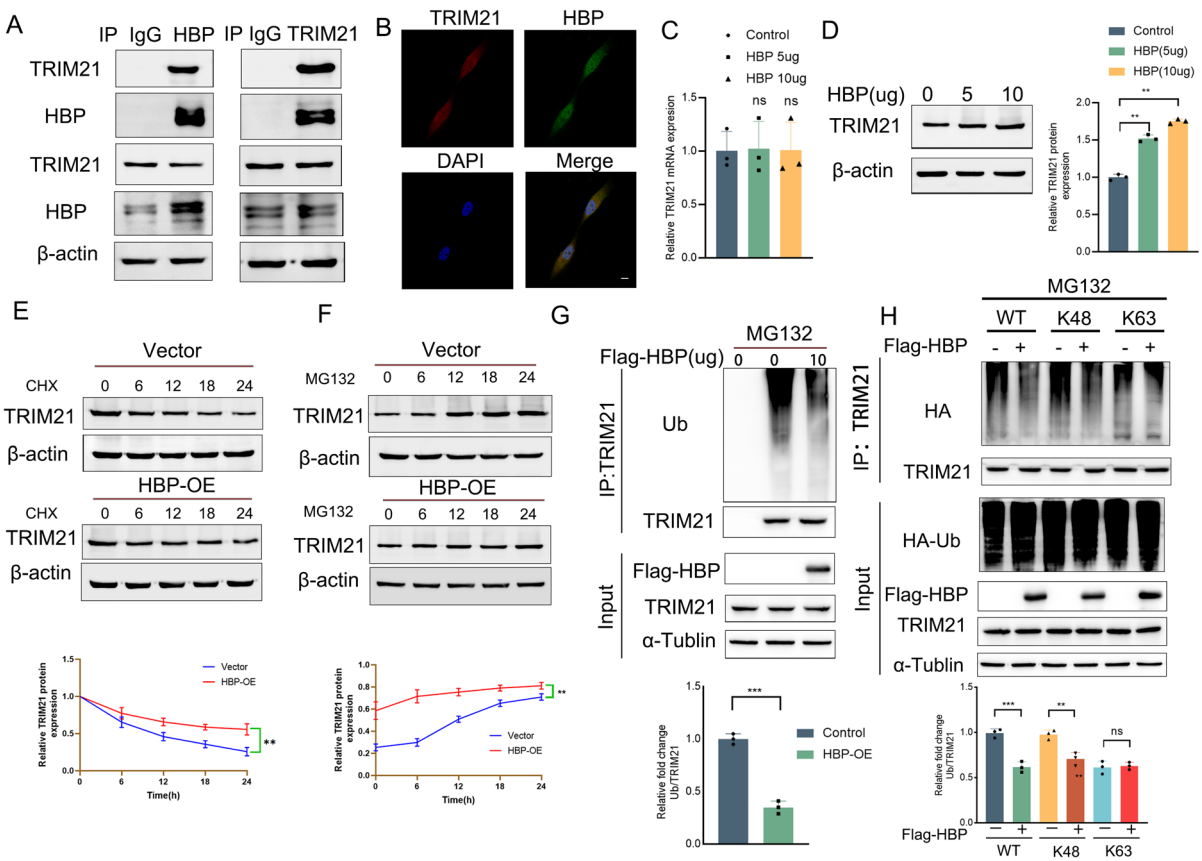


**Fig. 3** HBP interacts with TRIM21 and increases its protein stability. **A** Co-IP detection of HBP-TRIM21 binding in ECs treated with purified HBP. **B** Immunofluorescence showing co-localization of TRIM21 and HBP in the cytoplasm of ECs, scale bar: 10 μm. **C,D** mRNA and protein levels of TRIM21 in ECs overexpressing HBP. Data are represented as mean ± SD, n = 3, $^{**}P < 0.01$, ns $P > 0.05$. **E** CHX treatments to analyze TRIM21 stability and degradation in HBP-overexpressing ECs. Data are represented as mean ± SD, n = 3, $^{**}P < 0.01$. **F** Effects of MG132 on TRIM21 expression in HBP overexpression ECs. Data are represented as mean ± SD, n = 3, $^{**}P < 0.01$. **G** Ubiquitination levels of TRIM21 in HBP overexpression ECs treated with MG132 (10 μM) for 12 h. Data are represented as mean ± SD, n = 3, $^{***}P < 0.001$. **H** HEK293T cells were co-transfected with either vector or Flag-HBP together with HA-Ub WT, and its mutants (HA-Ub K48 and HA-Ub K63) and treated with MG132 (20 μM) for 12 h to assess TRIM21 ubiquitination levels. Data are represented as mean ± SD, n = 3, $^{**}P < 0.01$, $^{***}P < 0.001$

MG132 further increased the effects of HBP on TRIM21 protein expression, indicating that HBP modulates TRIM21 stability via the proteasome pathway (Fig. 3F). In addition, overexpression of HBP reduced TRIM21 ubiquitination (Fig. 3G). To further investigate the specific type of ubiquitination mediated by HBP, we co-transfected HEK293T cells with Flag-HBP, HA-Ub WT, and its mutants (HA-Ub K48 and HA-Ub K63). Ubiquitination analysis demonstrated that HBP significantly inhibited K48-linked ubiquitination of TRIM21 but had no substantial effect on K63-linked ubiquitination levels (Fig. 3H). These results indicate that HBP enhances TRIM21 protein stability by inhibiting its K48-linked ubiquitination.

## Regulation of EC permeability and glycolysis by TRIM21

To determine the effects of TRIM21 on EC permeability and glycolysis, the effects of TRIM21 knockdown and overexpression were evaluated

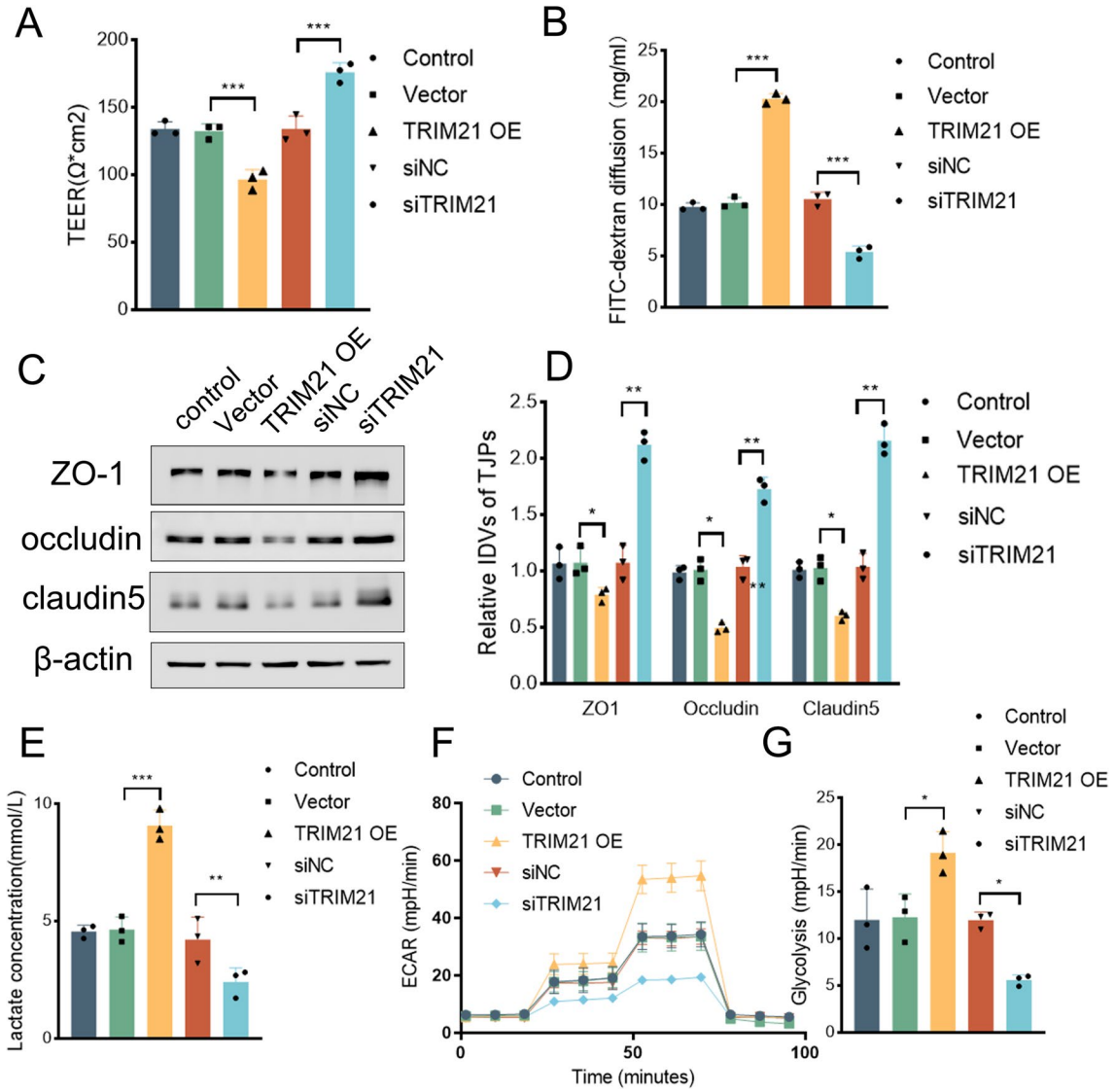


**Fig. 4** Role of TRIM21 in regulating EC permeability and glycolysis activity. **A, B** Influence of TRIM21 overexpression and knockdown on TEER values and FITC-dextran measurements in ECs. **C, D** Western blot analysis of tight junction proteins expression in ECs with TRIM21 overexpression and knockdown. Data are represented as mean ± SD, n = 3, $*P < 0.05$, $**P < 0.01$. **E–G** ECAR, lactate production, and glycolysis in ECs with altered TRIM21 expression. Data are represented as mean ± SD, n = 3, $*P < 0.05$, $**P < 0.01$, $***P < 0.001$

in HPMECs. Overexpression of TRIM21 significantly decreased TEER value and enhanced FITC–dextran leakage, indicating increased permeability. Conversely, TRIM21 knockdown increased TEER value and decreased FITC–dextran leakage, indicating improved barrier integrity (Fig. 4 A, B). In support of these results, the expression of ZO-1, occludin, and claudin-5 decreased in the TRIM21 overexpression group, while their levels increased after TRIM21 knockdown (Fig. 4C, D). Additionally, glycolytic activity and lactate production were markedly higher

in cells overexpressing TRIM21 and lower when TRIM21 was silenced (Fig. 4E-G). These results indicate that TRIM21 modulates endothelial barrier function and glycolytic activity.

## TRIM21 regulates EC permeability and glycolysis through P65 nuclear translocation

Previous studies have shown that TRIM21 promotes K63 ubiquitination of P65, which enhances P65 nuclear translocation in psoriasis (Yang et al. 2021). P65 is a crucial component of the NF-κB signaling pathway, regulating inflammatory processes and EC permeability and glycolysis through transcriptional regulation. Thus, we hypothesized that TRIM21 affects EC functions by modulating P65 nuclear translocation. Co-IP assays confirmed the endogenous interaction between TRIM21 and P65 in HPMECs (Fig. 5A). TRIM21 overexpression significantly increased the K63-linked ubiquitination of P65 (Fig. 5B) and P65 nuclear translocation (Fig. 5C, D). These results indicate that TRIM21-induced K63 ubiquitination facilitates P65 nuclear translocation in HPMECs. To determine if P65 nuclear translocation is involved in TRIM21 effects on HPMEC permeability and glycolysis, we employed JSH-23, a specific inhibitor of P65 nuclear translocation. JSH-23 reversed the decrease in TEER and increase in FITC–dextran leakage induced by TRIM21 overexpression in

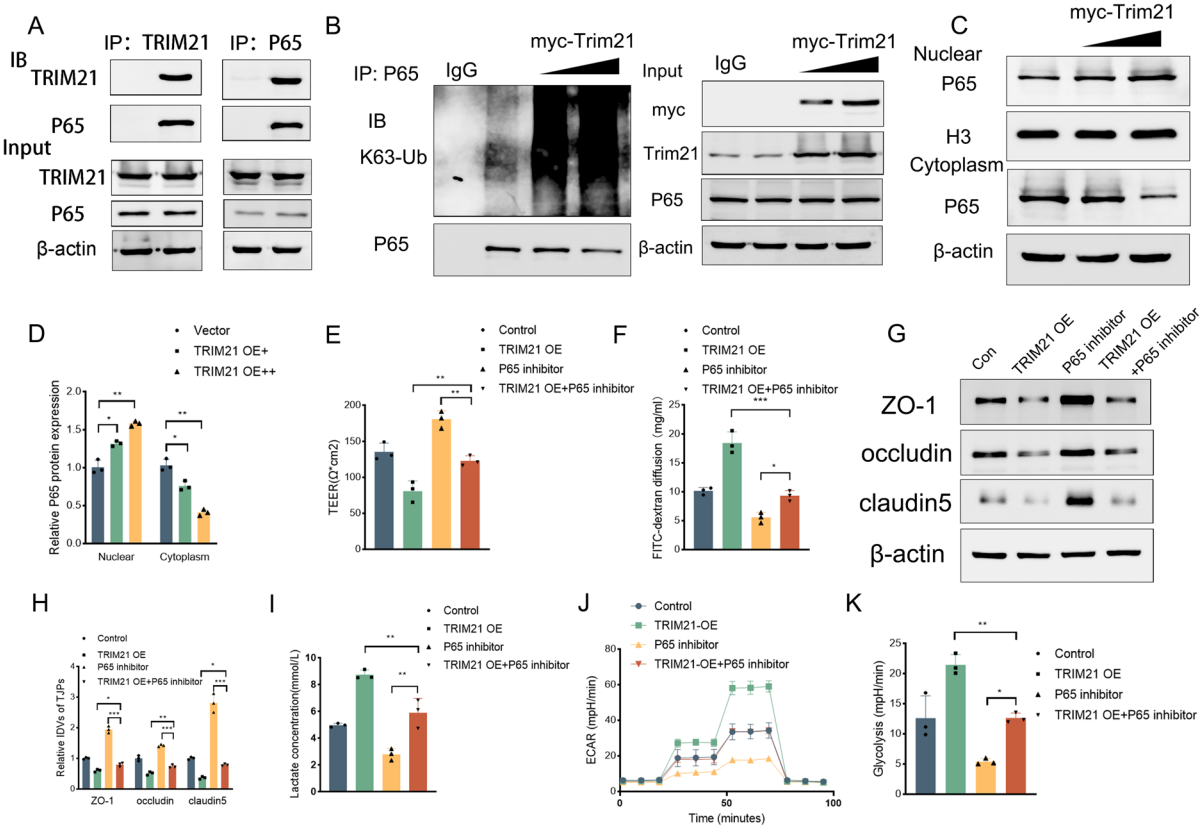


**Fig. 5** TRIM21 regulates endothelial functions through ubiquitination of P65. **A, B** TRIM21 binding and ubiquitination of P65 detected by Co-IP. **C, D** Effects of TRIM21 overexpression on P65 nuclear translocation. Data are represented as mean ± SD, n = 3, $^{*}P < 0.05$, $^{**}P < 0.01$. **E, F** The effects of TRIM21 overexpression and P65 inhibitor on TEER values and FITC-dextran measurements. **G, H** Effects of TRIM21 overexpression and P65 inhibitor on tight junction protein expression in ECs detected by Western blot. Data are represented as mean ± SD, n = 3, $^{*}P < 0.05$, $^{***}P < 0.001$. **I-K** ECAR, lactate production, and glycolysis assessed under the conditions of TRIM21 overexpression and P65 inhibitor. Data are represented as mean ± SD, n = 3, $^{*}P < 0.05$, $^{**}P < 0.01$

ECs (Fig. 5E, F). The expression of ZO-1, occludin, and claudin-5 proteins increased significantly in the TRIM21 overexpression + P65 inhibitor group compared to the TRIM21 overexpression group (Fig. 5G, H). Moreover, JSH-23 restored the upregulation of glycolytic capacity and lactate levels caused by TRIM21 overexpression in HPMECs (Fig. 5I-K). These results confirm that TRIM21 regulates HPMEC permeability and glycolysis via P65 nuclear translocation, suggesting that the endothelial regulatory pathways can be targeted.

## HBP enhances the interaction between TRIM21 and P65, regulating EC permeability and glycolysis through TRIM21-mediated ubiquitination of P65

HBP interacts with TRIM21, which interacts with P65 in HPMECs. Thus, we hypothesized that HBP modulates the interaction between TRIM21 and P65. As expected, the Co-IP experiments revealed that both recombinant HBP and sepsis-derived PMNs significantly enhance the endogenous interaction between TRIM21 and P65 (Fig. 6A). Thus, HBP

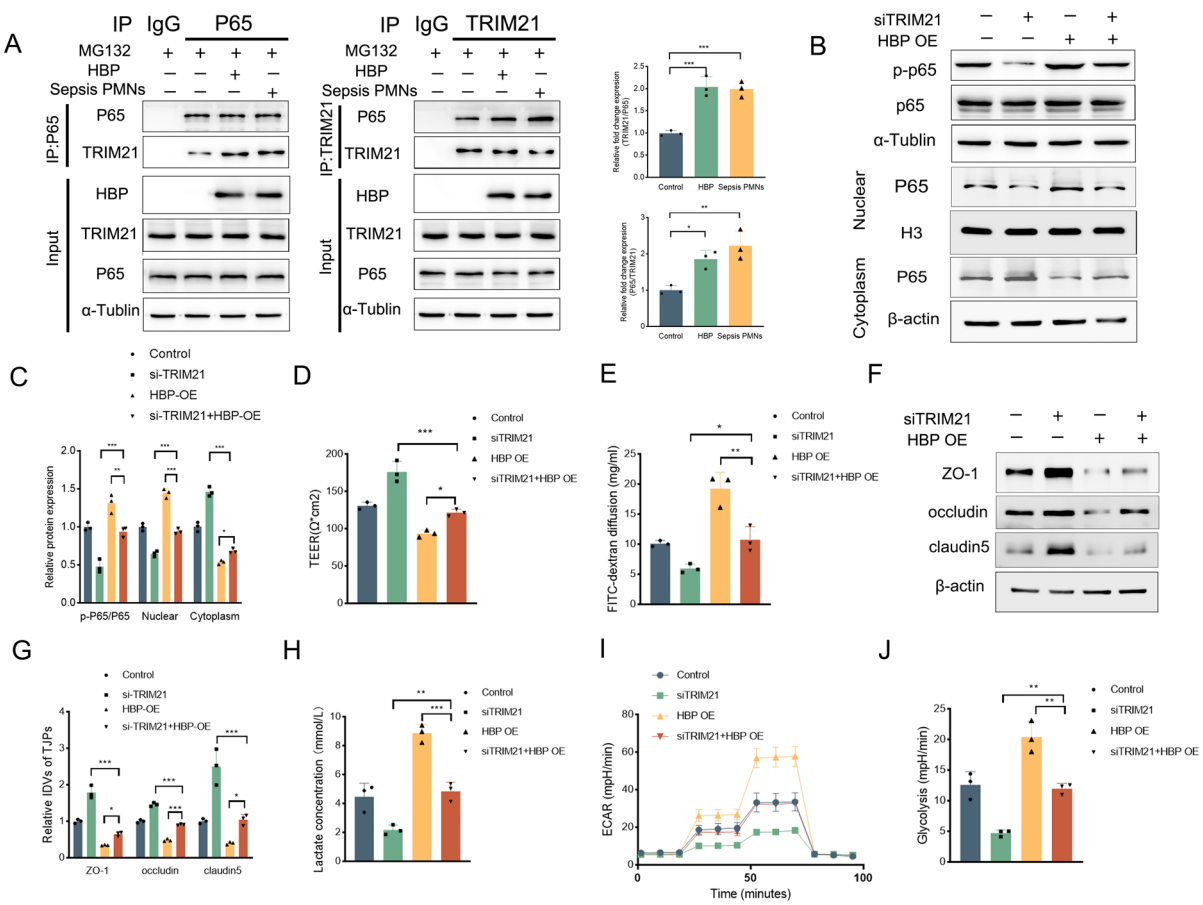


**Fig. 6** HBP promotes the interaction between TRIM21 and P65, and regulates endothelial cell permeability and glycolysis through TRIM21-induced ubiquitination of P65. **A** The effect of recombinant HBP and sepsis-derived PMNs on the interaction between TRIM21 and P65. Data are represented as mean ± SD, n = 3, $^{*}P < 0.05$, $^{**}P < 0.01$, $^{***}P < 0.001$. **B, C** Impact of HBP overexpression and TRIM21 knockdown on P65 phosphorylation and nuclear translocation. Data are represented as mean ± SD, n = 3, $^{*}P < 0.05$, $^{**}P < 0.01$, $^{***}P < 0.001$. **D, E** The effects of HBP overexpression and knockdown TRIM21 on TEER values and FITC-dextran measurements. **F, G** Western blot detects the effects of HBP overexpression and knockdown TRIM21 on tight junction protein expression in ECs. Data are represented as mean ± SD, n = 3, $^{*}P < 0.05$, $^{***}P < 0.001$. **H-J** ECAR, lactate production, and glycolysis in ECs with altered HBP and TRIM21 expression. Data are represented as mean ± SD, n = 3, $^{**}P < 0.01$, $^{***}P < 0.001$

strengthens the interaction between TRIM21 and P65. To explore the role of TRIM21-P65 in HBP-mediated effects on permeability and glycolysis, HPMECs overexpressing HBP were transfected with TRIM21 siRNA. SiTRIM21 reduced the phosphorylation of P65 and the nuclear translocation of P65 caused by HBP overexpression (Fig. 6B, C). Furthermore, qRT-PCR analysis of P65 downstream inflammatory factors (IL-6 and IL-1β) revealed that TRIM21 knockdown suppressed their upregulation induced by HBP overexpression (sFig 5A,B), confirming the dependency of HBP-mediated P65 activation on TRIM21. Building on previous findings that high-dose HBP activates the Rho signaling pathway, we investigated Rho/ROCK pathway involvement in low-dose HBP-mediated signaling. Western blot analysis showed that low-dose HBP (1 ug/mL) did not activate Rho/ROCK but significantly increased P65 phosphorylation, peaking at 24 h (sFig 3A). In contrast, high-dose HBP (10 ug/mL) activated both P65 and Rho/ROCK, with maximal effects at 6 h (sFigure 3B). Functional assays revealed that low-dose HBP treatment (12–24 h) significantly reduced TEER values (sFigure 3C) and increased FITC-dextran permeability (sFigure 3D), correlating with the time-dependent increase in P65 phosphorylation levels. These results suggest that low-dose HBP primarily exerts its effects via the P65 pathway rather than Rho/ROCK. Next, we investigated whether HBP-mediated P65 activation is dependent on TRIM21. Notably, TEER value increased and FITC–dextran leakage decreased in the HBP overexpression + siTRIM21 group compared to the HBP overexpression group (Fig. 6D, E). Importantly, siTRIM21 restored the expression of ZO-1, occludin, and claudin-5 (Fig. 6F, G). TRIM21 knockdown mitigated the increased glycolytic capacity and lactate levels prompted by HBP overexpression (Fig. 6H-J). These results confirmed that HBP facilitates interactions between TRIM21 and P65 and influences HPMEC permeability and glycolysis via TRIM21-mediated ubiquitination of P65.

## Silencing of TRIM21 reverses HBP-induced lung injury in vivo

In vitro experiments have confirmed the regulatory relationship between HBP, TRIM21, and P65; however, whether this regulation is consistent in the HBP-induced lung injury model remains unclear. Therefore, we further examined the expression and ubiquitination levels of TRIM21 and P65 in the lungs of HBP-treated mice. The results showed that TRIM21 expression was increased, while P65 expression remained unchanged in lung primary endothelial cells from HBP-treated mice (Fig. 7A). Ubiquitination assays revealed a decrease in TRIM21 ubiquitination levels (Fig. 7B)and a significant reduction in K63 ubiquitination of P65 (Fig. 7C) in the lung tissue of HBP-treated mice. In vivo experimental data further confirmed that the changes in the HBP-TRIM21-P65 signaling axis were consistent with the in vitro experimental results. Additionally, BALF from the HBP model mice showed a significant increase in neutrophil content (Fig. 7D), suggesting that HBP exacerbates neutrophil infiltration.

To ascertain the role of TRIM21 in HBP-induced lung injury in vivo, we utilized AAV6 vectors expressing either shRNA targeting TRIM21 (sh-TRIM21) or a nontargeting control (sh-NC). The vectors were administered intratracheally to C57/BL mice. TRIM21 expression decreased in lung primary endothelial cells of mice treated with sh-TRIM21 4 weeks after adenoviral infection (Fig. 7E). Subsequent administration of HBP via tail vein injection induced similar pathological changes in the lungs of wild type or AAV6 sh-NC mice. However, TRIM21 knockdown significantly mitigated the pulmonary pathological damage induced by HBP (Fig. 7F, G). Additionally, lung W/D ratios and Evans blue leakage were substantially reduced in TRIM21 knockdown mice compared to the sh-NC group (Fig. 7H, I). Lactate levels in BALF from TRIM21 knockdown mice were also significantly decreased compared to the sh-NC group (Fig. 7J). These results confirm that knocking down TRIM21 reverses lung injury triggered by HBP and are consistent with the ex vitro experiments. To further elucidate the role of TRIM21 in lung injury, we developed an LPS-induced lung injury model. Western blot analysis revealed a marked increase in TRIM21 expression in primary pulmonary endothelial cells from LPS-exposed mice (sFig 6A). Following TRIM21 knockdown and subsequent LPS challenge, HE staining demonstrated a significant attenuation of lung tissue damage (sFig 6B). These results indicate that

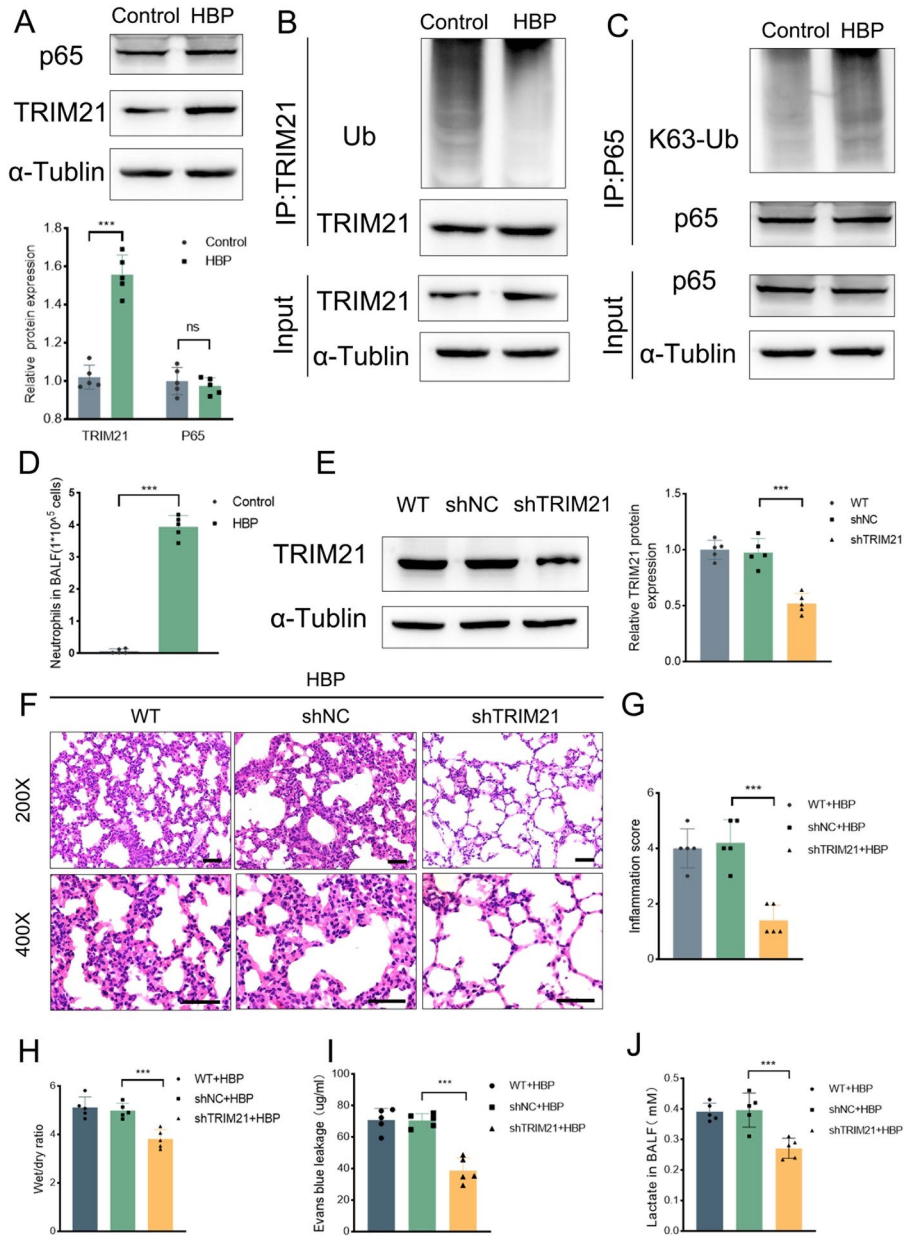


**Fig. 7** In vivo experiments confirm that silencing TRIM21 reverses HBP-induced lung injury.**A,** TRIM21 and P65 expression in the lung primary endothelial cells from mice treated with HBP. Data are represented as mean ± SD, n = 5, ***$P < 0.001$,ns, not significant. **B,C** Ubiquitination levels of TRIM21 and P65 in the lung tissues of mice treated with HBP. **D** Neutrophil count in BALF of mice treated with HBP. Data are represented as mean ± SD, n = 5, ***$P < 0.001$.**E** TRIM21 expression in the lung primary endothelial cells of sh-NC and sh-TRIM21 mice detected by Western blot. Data are represented as mean ± SD, n = 5, ***$P < 0.001$. **F,G** Lung tissues HE staining and lung inflammation score of sh-NC and sh-TRIM21 mice following HBP exposure, scale bar: 50 μm. Data are represented as mean ± SD, n = 5, ***$P < 0.001$. **H-J** Measurements of lung W/D ratio, Evans Blue leakage, and BALF lactate in sh-NC and sh-TRIM21 mice exposed to HBP. Data are represented as mean ± SD, n = 5, **$P < 0.01$, ***$P < 0.001$

TRIM21 may be critically involved in lung injury triggered by diverse etiological factors.

## Discussion

This study elucidates the pivotal role of the HBP/TRIM21/P65 axis in regulating pulmonary endothelial barrier function and metabolic reprogramming during sepsis. Mechanistically, HBP binds to TRIM21, inhibiting K48 ubiquitination and promoting TRIM21 expression. Importantly, HBP enhances the interaction between TRIM21 and P65, facilitating P65 phosphorylation and its nuclear translocation. This interaction forms a positive feedback loop that amplifies NF-κB signaling. Both in vitro and in vivo knockdown of TRIM21 effectively reversed HBP-induced increases in permeability and glycolysis,

thereby mitigating lung injury. These findings suggest that targeting TRIM21 may offer a potential therapeutic strategy for alleviating acute lung injury.

Neutrophil–endothelial cell interactions are involved in the progression of sepsis-induced lung injury (Liu et al. 2023). Activated neutrophils cause tissue injury and organ dysfunction by releasing cytokines, bioactive peptides, and enzymes during sepsis (Park et al. 2019; Wang et al. 2022a). In addition, HPMECs are involved in the development of ALI through increased vascular permeability, inflammatory responses, endothelial dysfunction, and pulmonary microthrombosis (Qiao et al. 2024). Tight junctions are necessary for the lung endothelial barrier function, and disruption of tight junctions results in ALI. In addition, aberrant glycolysis is associated with increased vascular permeability (Clyne 2021). For instance, lactate produced from glycolysis activates ERK, which stimulates calpain1/2. This activation leads to the proteolytic cleavage of VE-cadherin, a key protein in maintaining endothelial cohesion. Cleavage of VE-cadherin promotes its endocytosis in ECs during sepsis (Yang et al. 2022). In the present study, we focused on the effect of neutrophils on HPMEC permeability and glycolysis during sepsis. The coculture experiments showed that sepsis-induced PMNs altered HPMEC permeability and integrity and enhanced HPMECs glycolysis.

HBP is part of the serine protease family but lacks enzymatic activity due to substitutions in key serine and histidine residues at its active site. HBP is highly expressed in neutrophils but is virtually absent in ECs (Linder et al. 2010). HBP is sequestered in the secretory vesicles and azurophilic granules of neutrophils under physiological conditions and is released into the plasma upon neutrophil activation during sepsis (Fisher and Linder 2017). Consistent with other clinical studies (Hovold et al. 2018; McAuley et al. 2013), we demonstrated a correlation between plasma HBP levels and sepsis-induced lung injury. HBP is increased in supernatants from HPMECs cocultured with sepsis PMNs. Therefore, we hypothesize that HBP may be an important signal from neutrophils that modulates HPMEC permeability and glycolysis. Unfractionated heparin, which inhibits HBP, reversed the effects of sepsis PMNs on endothelial cell permeability and glycolysis, confirming the role of PMN-derived HBP in mediating PMN effects on HPMEC permeability and glycolysis. Our group and others reported that 10 ug/ml HBP increases the permeability of HPMECs at 6 h in vitro (Liu et al. 2022). However, the in vivo concentration of HBP that affects HPMEC permeability and glycolysis is unclear. In this study, 1 ug/ml HBP, near the plasma concentration in septic patients, increases HPMEC permeability and glycolysis in vitro at 24 h. Consistent with the in vitro experimental results, purified HBP protein, delivered via tail vein injection, induces ALI. Our findings demonstrate that the temporal effects of HBP on endothelial function are dose-dependent, with prolonged exposure to lower HBP concentrations exhibiting more pronounced regulatory effects on barrier function. HBP probably enters cells through endocytosis (Bentzer et al. 2016). Thus we hypothesized that HBP interacts with intracellular proteins in HPMECs. Coimmunoprecipitation and mass spectrometry analysis revealed that HBP interacts with TRIM21. Interestingly, HBP upregulated TRIM21 expression without altering mRNA expression, suggesting that HBP affects protein stability. Subsequent experiments with CHX and Mg132 demonstrated that HBP enhances TRIM21 protein stability through suppression of ubiquitin–proteasome-mediated degradation Ubiquitination analysis further revealed that HBP specifically suppressed K48-linked polyubiquitination of TRIM21, while exerting minimal impact on K63-linked ubiquitination patterns. This is the first study demonstrating that the secretory protein HBP interacts with TRIM21 and reduces the K48 ubiquitination and degradation of TRIM21.

TRIM21 was originally identified as an autoantigen involved in autoimmune diseases such as rheumatoid arthritis, systemic lupus erythematosus, and Sjogren's syndrome (Holwek et al. 2023; Jones et al. 2021). TRIM21 is downregulated in LPS-induced lung injury models, and overexpression of TRIM21 can alleviate LPS-induced inflammatory responses (Li et al. 2019). In contrast, proteomic analyses of plasma revealed significant elevations of TRIM21 in individuals with bacterial community-acquired pneumonia. Thus, TRIM21 is a predictive biomarker for bacterial community-acquired pneumonia (Palma Medina et al. 2023). These contradictory findings suggest that the role of TRIM21 in ALI may be bidirectional. The expression and function of TRIM21 may be associated with specific injury factors, the severity of the disease, and different stages of the illness. Our results showed that TRIM21 significantly

increases HPMEC permeability and promotes glycolysis activity. Moreover, TRIM21, functioning as a ubiquitin E3 ligase, modulates various biological pathways through the ubiquitination of substrates, including established targets such as IRF3, IRF7, IRF8, P65, and PHB1 (Foss et al. 2019; Li et al. 2023b). Among the substrates, P65, a key component of the NF-κB pathway, is recognized as a pivotal regulator of inflammation and immune responses in ALI (Xiao et al. 2020). NF-κB mediates neutrophil adhesion to ECs, alters endothelial permeability, activates intravascular coagulation, and drives metabolic reprogramming in ECs. In psoriasis, TRIM21 mediates K63-linked ubiquitination of P65, which elevates P65 phosphorylation levels and promotes its translocation into the nucleus, thereby enhancing its transcriptional function.(Yang et al. 2021). P65 translocation is a crucial step in NF-κB activation, leading to the transcription of target genes involved in various cellular responses (Xing et al. 2023). Our results demonstrate that TRIM21 binds to and promotes K63-linked ubiquitination of P65, facilitating its nuclear translocation. Inhibition of P65 nuclear translocation reverses the effects of TRIM21 on HPMEC permeability and glycolysis.

Protein–protein interactions influence protein stability, activity, subcellular localization, and interactions with other molecules (Majolee et al. 2019; Shang et al. 2022; Wang et al. 2022b). Building on the observed interaction between HBP and TRIM21, we hypothesized that HBP may regulate TRIM21 binding to P65. Our results show that both recombinant HBP and sepsis-derived PMNs enhances the interaction between TRIM21 and P65, confirming the role of endogenous HBP in facilitating this interaction. The classic mechanism for high-dose(10 ug/mL) HBP regulation of EC permeability includes the activation of PKC and Rho kinase, leading to calcium-dependent cytoskeletal rearrangement and cell contraction (Gautam et al. 2001). High-dose HBP also activates the TGFβ2-smad2/3 signal pathway and modulates the cytoskeleton and permeability (Liu et al. 2022). This study revealed that low-dose HBP selectively activates P65 without inducing Rho signaling pathway activation, demonstrating a dose-dependent divergence in HBP-mediated signaling pathways. Furthermore, the regulation of P65 phosphorylation and nuclear translocation by HBP was shown to be TRIM21-dependent. However, the modulation of HPMEC permeability and glycolysis by HBP through the TRIM21-P65 axis was unclear. In both in vitro and in vivo experiments, TRIM21 knockdown reversed the increased HPMEC permeability and glycolysis mediated by HBP. Nevertheless, the knockdown of TRIM21 did not fully reverse the effects of HBP on permeability and glycolysis, suggesting that, in addition to TRIM21, HBP may regulate these processes through other molecular mechanisms that warrant further investigation. These findings unveil a novel regulatory mechanism in which HBP regulates HPMEC permeability and glycolysis through modulation of the TRIM21-P65 interaction, with the effect dependent on TRIM21-dependent ubiquitination of P65.

Our study has several limitations. First, as mice do not naturally express HBP protein, we administered purified HBP protein intravenously to establish the experimental model. This approach differs significantly from the cecal ligation and puncture (CLP) model of sepsis, which more closely mimics the progression of human sepsis by representing multiple pathogenic factors (Ruiz et al. 2016). A potentially more relevant model involves the use of HBP knock-in mice combined with the CLP model to study HBP function in vivo more effectively. Second, we used unfractionated heparin as a non-specific inhibitor of HBP. However, an HBP-neutralizing antibody may offer a more targeted inhibition. Third, our current study does not clarify the binding domains and sites between HBP and TRIM21 due to limitations in our experimental conditions. Further research is required to elucidate these interactions and to determine whether HBP concurrently interacts with TRIM21 and P65. Fourth, the adenovirus infection used in this study targeted lung tissue broadly rather than specifically infecting vascular endothelial cells. This lack of cell-type specificity is a limitation of our approach. The use of endothelial cell-specific conditional knockout mice would be a more precise and suitable model to address this issue.

In conclusion, our findings demonstrate that septic PMNs contribute to ALI by increasing HPMEC permeability and glycolysis through the secretion of HBP. This study is the first to show that HBP interacts with TRIM21, enhancing its protein stability by preventing K48 ubiquitination-mediated degradation, thereby increasing TRIM21 protein levels. TRIM21 mediates K63-linked ubiquitination of P65,

promoting its nuclear translocation, which in turn increases both HPMEC permeability and glycolysis. Additionally, HBP not only stabilizes TRIM21 but also enhances the interaction between TRIM21 and P65, modulating endothelial functions through the TRIM21-P65 pathway. This is the first investigation to elucidate the molecular interplay within the HBP-TRIM21-P65 signaling axis in ALI, suggesting that targeting the HBP-TRIM21-P65 signaling axis may provide a novel therapeutic strategy for acute lung injury.

**Acknowledgements** We thank Professor Liu Cao (The College of Basic Medical Science, Health Sciences Institute, China Medical University, Shenyang, Liaoning Province 110122, China) for his valuable advice and support during the course of this study.

**Author contribution** Xiaochun Ma developed the study concept and supervised this project. Jian Zhang, completed most of the experiments and thesis writing. Jian Zhang, Yong Cao and Senxiao Dong performed the in-vivo essay. Wenqi Shu participated in the in-vitro experiments and the analysis of experimental data. Yini Sun participate in designing the experimental idea and revised the writing. All authors read and approved the final manuscript.

**Funding** This work was supported by grants from Nature and Science Foundation of China (82172130, 2021YFC2500805).

**Data availability** No datasets were generated or analysed during the current study.

**Declarations**

**Ethical approval** All clinical data collection and experiments were conducted in accordance with the approval granted by the Ethics Committee of the First Affiliated Hospital of China Medical University (Approval Number: 2023–157). All animal procedures were approved by the Institutional Animal Care and Use Committee of China Medical University (Approval Number: KT20240002).

**Competing interests** The authors declare no competing interests.



## References

Alharbi KS, Fuloria NK, Fuloria S, Rahman SB, Al-Malki WH, Javed Shaikh MA, Thangavelu L, Singh SK, Rama Raju Allam VS, Jha NK, Chellappan DK, Dua K, Gupta G. Nuclear factor-kappa B and its role in inflammatory lung disease. Chem Biol Interact. 2021;345:109568. https://doi.org/10.1016/j.cbi.2021.109568.

Bellani G, Laffey JG, Pham T, Fan E, Brochard L, Esteban A, Gattinoni L, van Haren F, Larsson A, McAuley DF, Ranieri M, Rubenfeld G, Thompson BT, Wrigge H, Slutsky AS, Pesenti A, Investigators LS, Group ET. Epidemiology, Patterns of Care, and Mortality for Patients With Acute Respiratory Distress Syndrome in Intensive Care Units in 50 Countries. JAMA. 2016;315:788–800. https://doi.org/10.1001/jama.2016.0291.

Bentzer P, Fisher J, Kong HJ, Morgelin M, Boyd JH, Walley KR, Russell JA, Linder A. Heparin-binding protein is important for vascular leak in sepsis. Intensive Care Med Exp. 2016;4:33. https://doi.org/10.1186/s40635-016-0104-3.

Clyne AM. Endothelial response to glucose: dysfunction, metabolism, and transport. Biochem Soc Trans. 2021;49:313–25. https://doi.org/10.1042/BST20200611.

Dalal PJ, Muller WA, Sullivan DP. Endothelial Cell Calcium Signaling during Barrier Function and Inflammation. Am J Pathol. 2020;190:535–42. https://doi.org/10.1016/j.ajpath.2019.11.004.

Evans L, Rhodes A, Alhazzani W, Antonelli M, Coopersmith CM, French C, Machado FR, McIntyre L, Ostermann M, Prescott HC, Schorr C, Simpson S, Wiersinga WJ, Alshamsi F, Angus DC, Arabi Y, Azevedo L, Beale R, Beilman G, Belley-Cote E, Burry L, Cecconi M, Centofanti J, Coz Yataco A, De Waele J, Dellinger RP, Doi K, Du B, Estenssoro E, Ferrer R, Gomersall C, Hodgson C, Moller MH, Iwashyna T, Jacob S, Kleinpell R, Klompas M, Koh Y, Kumar A, Kwizera A, Lobo S, Masur H, McGloughlin S, Mehta S, Mehta Y, Mer M, Nunnally M, Oczkowski S, Osborn T, Papathanassoglou E, Perner A, Puskarich M, Roberts J, Schweickert W, Seckel M, Sevransky J, Sprung CL, Welte T, Zimmerman J, Levy M. Surviving sepsis campaign: international guidelines for management of sepsis and septic shock 2021. Intensive Care Med. 2021;47:1181–247. https://doi.org/10.1007/s00134-021-06506-y.

Fisher J, Linder A. Heparin-binding protein: a key player in the pathophysiology of organ dysfunction in sepsis. J

Intern Med. 2017;281:562–74. https://doi.org/10.1111/joim.12604.

Foss S, Bottermann M, Jonsson A, Sandlie I, James LC, Andersen JT. TRIM21-From Intracellular Immunity to Therapy. Front Immunol. 2019;10:2049. https://doi.org/10.3389/fimmu.2019.02049.

Gao W, Li Y, Liu X, Wang S, Mei P, Chen Z, Liu K, Li S, Xu XW, Gan J, Wu J, Ji C, Ding C, Liu X, Lai Y, He HH, Lieberman J, Wu H, Chen X, Li J. TRIM21 regulates pyroptotic cell death by promoting Gasdermin D oligomerization. Cell Death Differ. 2022;29:439–50. https://doi.org/10.1038/s41418-021-00867-z.

Gautam N, Olofsson AM, Herwald H, Iversen LF, Lundgren-Akerlund E, Hedqvist P, Arfors KE, Flodgaard H, Lindbom L. Heparin-binding protein (HBP/CAP37): a missing link in neutrophil-evoked alteration of vascular permeability. Nat Med. 2001;7:1123–7. https://doi.org/10.1038/nm1001-1123.

Holwek E, Opinc-Rosiak A, Sarnik J, Makowska J. Ro52/TRIM21 - From host defense to autoimmunity. Cell Immunol. 2023;393–394:104776. https://doi.org/10.1016/j.cellimm.2023.104776.

Hovold G, Palmcrantz V, Kahn F, Egesten A, Pahlman LI. Heparin-binding protein in sputum as a marker of pulmonary inflammation, lung function, and bacterial load in children with cystic fibrosis. BMC Pulm Med. 2018;18:104. https://doi.org/10.1186/s12890-018-0668-7.

Joffre J, Hellman J, Ince C, Ait-Oufella H. Endothelial Responses in Sepsis. Am J Respir Crit Care Med. 2020;202:361–70. https://doi.org/10.1164/rccm.201910-1911TR.

Jones EL, Laidlaw SM, Dustin LB. TRIM21/Ro52 - Roles in Innate Immunity and Autoimmune Disease. Front Immunol. 2021;12:738473. https://doi.org/10.3389/fimmu.2021.738473.

Li L, Wei J, Mallampalli RK, Zhao Y, Zhao J. TRIM21 Mitigates Human Lung Microvascular Endothelial Cells' Inflammatory Responses to LPS. Am J Respir Cell Mol Biol. 2019;61:776–85. https://doi.org/10.1165/rcmb.2018-0366OC.

Li D, Yang L, Wang W, Song C, Xiong R, Pan S, Li N, Geng Q. Eriocitrin attenuates sepsis-induced acute lung injury in mice by regulating MKP1/MAPK pathway mediated-glycolysis. Int Immunopharmacol. 2023a;118:110021. https://doi.org/10.1016/j.intimp.2023.110021.

Li X, Yang L, Chen S, Zheng J, Zhang H, Ren L. Multiple Roles of TRIM21 in Virus Infection. Int J Mol Sci. 2023b;24:1683. https://doi.org/10.3390/ijms24021683.

Linder A, Soehnlein O, Akesson P. Roles of heparin-binding protein in bacterial infections. J Innate Immun. 2010;2:431–8. https://doi.org/10.1159/000314853.

Liu Z, Chen M, Sun Y, Li X, Cao L, Ma X. Transforming growth factor-beta receptor type 2 is required for heparin-binding protein-induced acute lung injury and vascular leakage for transforming growth factor-beta/Smad/Rho signaling pathway activation. FASEB J. 2022;36:e22580. https://doi.org/10.1096/fj.202200228RRRRR.

Liu D, Langston JC, Prabhakarpandian B, Kiani MF, Kilpatrick LE. The critical role of neutrophil-endothelial cell interactions in sepsis: new synergistic approaches employing organ-on-chip, omics, immune cell phenotyping and in silico modeling to identify new therapeutics. Front Cell Infect Microbiol. 2023;13:1274842. https://doi.org/10.3389/fcimb.2023.1274842.

Lu Z, Li X, Yang P, Mu G, He L, Song C, Xu F. Heparin-Binding Protein Enhances NF-kappaB Pathway-Mediated Inflammatory Gene Transcription in M1 Macrophages via Lactate. Inflammation. 2021;44:48–56. https://doi.org/10.1007/s10753-020-01263-4.

Majolee J, Kovacevic I, Hordijk PL. Ubiquitin-based modifications in endothelial cell-cell contact and inflammation. J Cell Sci. 2019;132. https://doi.org/10.1242/jcs.227728

Marziano C, Genet G, Hirschi KK. Vascular endothelial cell specification in health and disease. Angiogenesis. 2021;24:213–36. https://doi.org/10.1007/s10456-021-09785-7.

McAuley DF, O'Kane CM, Craig TR, Shyamsundar M, Herwald H, Dib K. Simvastatin decreases the level of heparin-binding protein in patients with acute lung injury. BMC Pulm Med. 2013;13:47. https://doi.org/10.1186/1471-2466-13-47.

Meyer NJ, Gattinoni L, Calfee CS. Acute respiratory distress syndrome. Lancet. 2021;398:622–37. https://doi.org/10.1016/S0140-6736(21)00439-6.

Millar MW, Fazal F, Rahman A. Therapeutic Targeting of NF-kappaB in Acute Lung Injury: A Double-Edged Sword. Cells. 2022;11. https://doi.org/10.3390/cells11203317

Palma Medina LM, Babacic H, Dzidic M, Parke A, Garcia M, Maleki KT, Unge C, Lourda M, Kvedaraite E, Chen P, Muvva JR, Cornillet M, Emgard J, Moll K, Karolinska KIKC-SG, Michaelsson J, Flodstrom-Tullberg M, Brighenti S, Buggert M, Mjosberg J, Malmberg KJ, Sandberg JK, Gredmark-Russ S, Rooyackers O, Svensson M, Chambers BJ, Eriksson LI, Pernemalm M, Bjorkstrom NK, Aleman S, Ljunggren HG, Klingstrom J, Stralin K, Norrby-Teglund A. Targeted plasma proteomics reveals signatures discriminating COVID-19 from sepsis with pneumonia. Respir Res. 2023;24:62. https://doi.org/10.1186/s12931-023-02364-y.

Park I, Kim M, Choe K, Song E, Seo H, Hwang Y, Ahn J, Lee SH, Lee JH, Jo YH, Kim K, Koh GY, Kim P. Neutrophils disturb pulmonary microcirculation in sepsis-induced acute lung injury. Eur Respir J. 2019;53. https://doi.org/10.1183/13993003.00786-2018

Qiao X, Yin J, Zheng Z, Li L, Feng X. Endothelial cell dynamics in sepsis-induced acute lung injury and acute respiratory distress syndrome: pathogenesis and therapeutic implications. Cell Commun Signal. 2024;22:241. https://doi.org/10.1186/s12964-024-01620-y.

Ruiz S, Vardon-Bounes F, Merlet-Dupuy V, Conil JM, Buleon M, Fourcade O, Tack I, Minville V. Sepsis modeling in mice: ligation length is a major severity factor in cecal ligation and puncture. Intensive Care Med Exp. 2016;4:22. https://doi.org/10.1186/s40635-016-0096-z.

Shang S, Liu J, Hua F. Protein acylation: mechanisms, biological functions and therapeutic targets. Signal Transduct Target Ther. 2022;7:396. https://doi.org/10.1038/s41392-022-01245-y.

Wang K, Wang M, Liao X, Gao S, Hua J, Wu X, Guo Q, Xu W, Sun J, He Y, Li Q, Gao W. Locally organised and

activated Fth1(hi) neutrophils aggravate inflammation of acute lung injury in an IL-10-dependent manner. Nat Commun. 2022a;13:7703. https://doi.org/10.1038/s41467-022-35492-y.

Wang S, Osgood AO, Chatterjee A. Uncovering post-translational modification-associated protein-protein interactions. Curr Opin Struct Biol. 2022b;74:102352. https://doi.org/10.1016/j.sbi.2022.102352.

Xiao K, He W, Guan W, Hou F, Yan P, Xu J, Zhou T, Liu Y, Xie L. Mesenchymal stem cells reverse EMT process through blocking the activation of NF-kappaB and Hedgehog pathways in LPS-induced acute lung injury. Cell Death Dis. 2020;11:863. https://doi.org/10.1038/s41419-020-03034-3.

Xing Z, Zhen Y, Chen J, Du M, Li D, Liu R, Zheng J. KPNA2 Silencing, Regulated by E3 Ubiquitin Ligase FBXW7, Alleviates Endothelial Dysfunction and Inflammation Through Inhibiting the Nuclear Translocation of p65 and IRF3: A Possible Therapeutic Approach for Atherosclerosis. Inflammation. 2023;46:2071–88. https://doi.org/10.1007/s10753-023-01863-w.

Yang Y, Liu G, He Q, Shen J, Xu L, Zhu P, Zhao M. A Promising Candidate: Heparin-Binding Protein Steps onto the Stage of Sepsis Prediction. J Immunol Res. 2019;2019:7515346. https://doi.org/10.1155/2019/7515346.

Yang L, Zhang T, Zhang C, Xiao C, Bai X, Wang G. Upregulated E3 ligase tripartite motif-containing protein 21 in psoriatic epidermis ubiquitylates nuclear factor-kappaB p65 subunit and promotes inflammation in keratinocytes. Br J Dermatol. 2021;184:111–22. https://doi.org/10.1111/bjd.19057.

Yang K, Fan M, Wang X, Xu J, Wang Y, Gill PS, Ha T, Liu L, Hall JV, Williams DL, Li C. Lactate induces vascular permeability via disruption of VE-cadherin in endothelial cells during sepsis. Sci Adv. 2022;8:eabm8965. https://doi.org/10.1126/sciadv.abm8965.